

# Experimental methods in astroparticle physics

## SS2020

**Teresa Marrodán Undagoitia**

Max-Planck-Institut für Kernphysik,  
Saupfercheckweg 1, 69117 Heidelberg, Germany

E-mail: [marrodan@mpi-hd.mpg.de](mailto:marrodan@mpi-hd.mpg.de)

### Contents

<b>1</b>	<b>Lecture 1: Dark matter indications</b>	<b>2</b>
1.1	Dispersion velocities of galaxies in clusters . . . . .	2
1.2	Rotation curves . . . . .	2
1.3	Gravitational lensing . . . . .	3
1.4	Galaxy-cluster collisions . . . . .	5
1.5	Large structure formation . . . . .	6
1.6	Cosmic microwave background . . . . .	8
1.7	Summary . . . . .	10

## 1. Lecture 1: Dark matter indications

This lecture summarizes some of the indications from Astronomy and Cosmology of the existence of dark matter. Most of these hints come from observation of how gravitation acts differently than expected.

A useful analogy is the discovery of Neptune. The position of this planet was mathematically predicted before it was actually observed. Before the discovery of Neptune, irregularities had been seen in the trajectory of Uranus which could not be explained by Newton's laws. The irregularities could, however, be resolved if there would be another planet affecting its path. Observations towards the predicted position quickly lead to the discovery of the new planet. Similarly, the unexpected behaviour of astrophysical objects point us to the existence of additional matter. As it doesn't emit light, it is commonly called dark matter.

### *1.1. Dispersion velocities of galaxies in clusters*

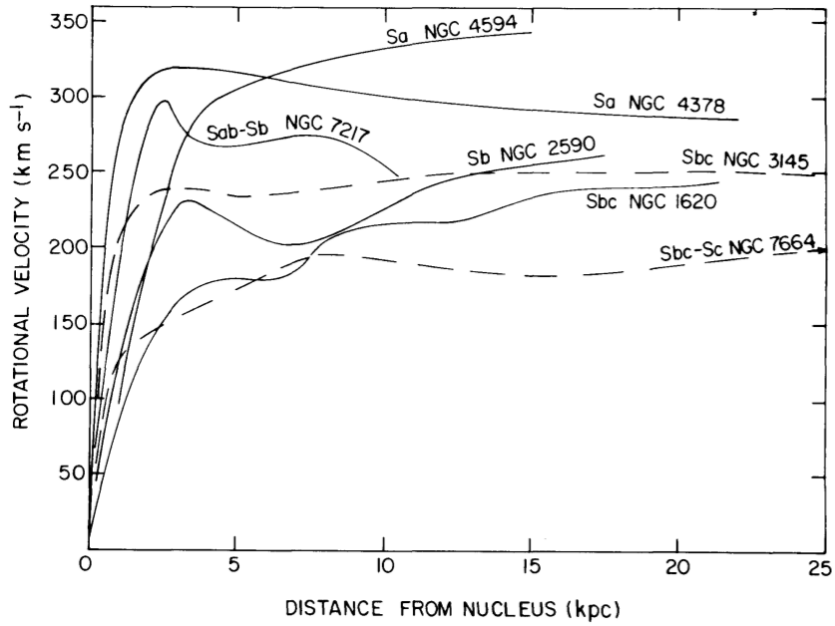
Historically, the first hints for dark matter arose from astronomical observations. The first evidence of dark matter in the present understanding was the measurement of unexpectedly high velocities of nebulae in the Coma cluster. This brought Fritz Zwicky [1] in 1933 to the idea that a large amount of dark matter could be the explanation for the unexpected high velocities. He employed the virial theorem which related the kinetic and potential energies of a stable system to infer masses in galaxy clusters as the Coma cluster. To reach the dispersion velocities observed, the mass of the Coma cluster would need to be  $\sim 400$  times larger than the observed one.

*Calculation in the exercises*

### *1.2. Rotation curves*

Another early indication for dark matter comes from the rotation curves of stars and gas clouds in galaxies. The rotation velocity is measured from the Doppler shift of the 21 cm hydrogen line. It is most precise in the innermost part of the Galaxies since the errors at large distances from the galaxy center become larger due to the absence of objects/signal. In 1978, Vera C. Rubin et al. [2] found that rotation velocities of stars in galaxies stay approximately constant with increasing distance to their galactic center (see figure 1). This observation was in contradiction with the expectation, as objects outside the visible mass distribution should have velocities  $v \propto \sqrt{1/r}$  following Newtonian dynamics. A uniformly-distributed halo of dark matter (with density  $\rho \propto 1/r^2$ ) could explain both the velocities in clusters and the rotation velocities of objects far from the luminous matter in galaxies.

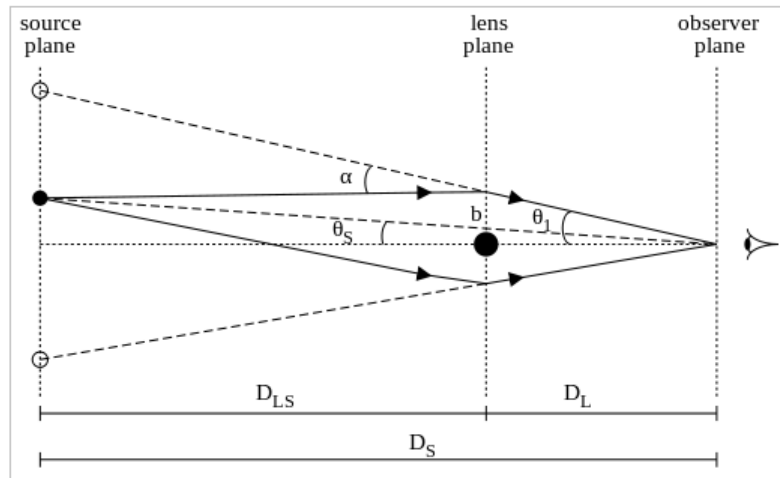
*Calculation in the exercises*



**Figure 1.** Examples of rotation curve measurements. Figure from V. Rubin *et al.*, 1978 [2].

### 1.3. Gravitational lensing

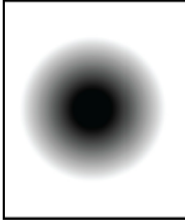


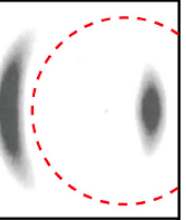
The gravitational lensing effect discussed by Albert Einstein [3] in 1936, occurs when a massive object is in the line of sight between the observer at the Earth and the object under study. The light-rays are deflected through their path due to the gravitational field resulting, for example, in multiple images or a deformation of the observable's image (see figure 2). The degree of deformation can be used to reconstruct the gravitational



**Figure 2.** Scheme of gravitational lensing effect, Figure from Lukovic et al. arXiv:1411.3556 [astro-ph.CO]

potential of the object that deflects the light along the line of sight. From various observations it has been found that the reconstructed mass using this method is greater than the luminous matter, resulting in very large mass to light ratios (from a few to hundreds).

There are different types of lensing [4]: strong, flexion, weak and microlensing. Figure 3 shows the classification of images from the first three lensing types. Strong

No lensing	Weak lensing	Flexion	Strong lensing
			
	Large-scale structure	Substructure, outskirts of halos	Cluster and galaxy cores

**Figure 3.** Various regimes of gravitational lensing image distortion. A circular source is distorted into an ellipse by weak lensing being the typical resulting axis ratio  $\sim 2\%$  (exaggerated for illustration). For most curved space-time (most massive objects), strong gravitational lensing produces multiple imaging and giant arcs. Figure from R. Massey *et al.* (2010), arXiv:1001.1739 [4].

lensing appears for dense concentrations of mass. If source exactly behind the lens, an Einstein rings can be observed, otherwise multiple images may result. Figure 4 displays a couple of examples of strong lensing.

*Strong lensing calculation in the exercises*



**Figure 4.** (Left) Strong lensing: Einstein ring. Figure from ESA/Hubble & NASA. (Right) Weak lensing in Abell 2218. Figure from NASA.

Weak lensing appears when the lines of sight pass through more extended objects. By analysing a large number of objects behind the lens, a statistical analysis can be performed to extract a mass distribution map. This technique is meanwhile standard to

determine the dark matter profile of different object. An example of this is the mapping of the mass distribution in galaxy-cluster collisions (see next section). Flexion is an intermediate effect between strong and weak lensing. Finally, microlensing is an effect in which a small increase in observed luminosity can be registered when a small object crosses the line of sight of a star. It is commonly used to search for Jupiter-like objects (this will be also discuss in the next lecture).

#### 1.4. Galaxy-cluster collisions

Galaxy clusters are gravitational bounded objects composed by stars in galaxies, gas clouds and dark matter. Although it is a rare process, a few collisions of galaxy clusters have been measured. Gravitational lensing has also been applied to this cases to reconstruct the mass distributions in such events where mass to light ratios of  $> 200$  are measured. In addition, an X-ray signal from the colliding gas cloud is also observed. For the cases in which the collision happens in a direction tangential to observers on Earth, gravitational lensing, X-rays and images in the visible from common telescopes provide great information to understand the dynamics in such collisions.

Three such examples are shown in figure 5: the blue regions represent the locations of high matter density as reconstructed via gravitational lensing and the reddish color arise from the X-ray signals. While the largest part of the visible mass (the gas clouds)



**Figure 5.** Galaxy-cluster collisions: bullet cluster, Abell 520 and DLSCL J0916.2+2951, respectively. Figures from NASA/CXC/M. Weiss - Chandra X-Ray Observatory: 1E 0657-56, X-ray: NASA / CXC/ U. Victoria/ A. Mahdavi et al. and arXiv:1110.4391.

collides producing X-rays at the collision spot, the stars and the dark matter cross through each other without mayor distortion. The gravitational lensing signal points that the majority of the mass is in the form of dark matter with no or very little self-interaction.

Like shown above, in several examples (see [5]) and in an extensive study of 72 cluster collisions [6], the reconstructed gravitational centers appear clearly separated from the main constituent of the ordinary matter, i.e. the gas clouds which collide and produce detectable X- rays. This can be interpreted as being due to dark matter haloes

that continue their trajectories independently of the collision. Figure 6 (from [6]) shows a cartoon showing the three components in each piece of substructure and their relative offsets, illustrated by black lines. The three components remain within a common gravitational potential, but their centroids become offset due to the different forces acting on them. On the right, the observed offsets between the three components for

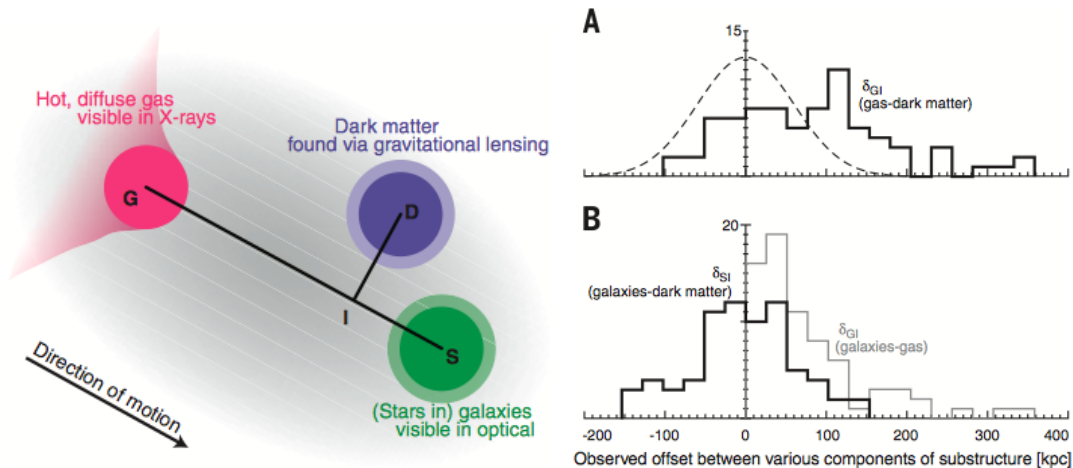


**Figure 6.** Galaxy-cluster collisions: (Right) Diagram of the displacement between gas (red), dark matter (blue) and the stars (green). (Left) Displacement results for 72 collisions. Figure from D. Harvey *et al.* Science 347 (2015) 1462, arXiv:1503.07675 [6].

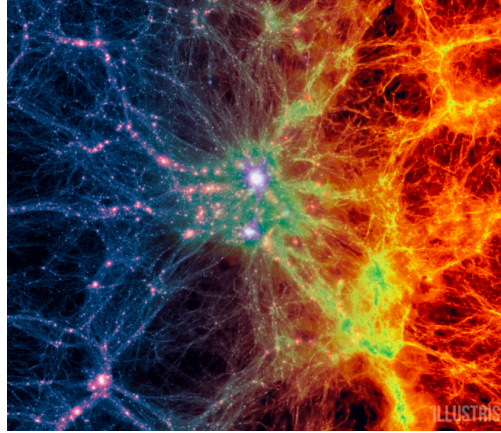
72 objects are shown. The offsets  $\delta_{SI}$  and  $\delta_{GI}$  consider the fact that gravitational lensing measures the total mass, not just that of dark matter. (A) The observed offset between gas and mass, in the direction of motion. The smooth dashed curve shows the distribution expected if dark matter would not exist. (B) Observed offsets from galaxies to other components well centered around zero. An upper limit to the self-interaction cross-section for dark matter can be derived from these observations.

### 1.5. Large structure formation

Currently, the information available on the large structures in our Universe comes from the cosmic microwave background maps, spectroscopic surveys, gravitational lensing and Lyman- $\alpha$  line measurements of quasars. In order to understand the formation of these matter distributions from the time of the CMB emission to the ones today, N-body simulations of dark matter particles have been carried out [7]. These simulations propagate particles using super computers aiming to describe the structure growth, producing a cosmic web ranging from  $\sim 10$  kpc objects to the largest scales. Meanwhile, this type of simulations reproduce very accurately the measurements made by galaxy surveys. Measurements of the Lyman- $\alpha$  forest and weak lensing confirm the cosmic structure considering not only galaxies and gas clouds but also non-luminous and non-baryonic matter.

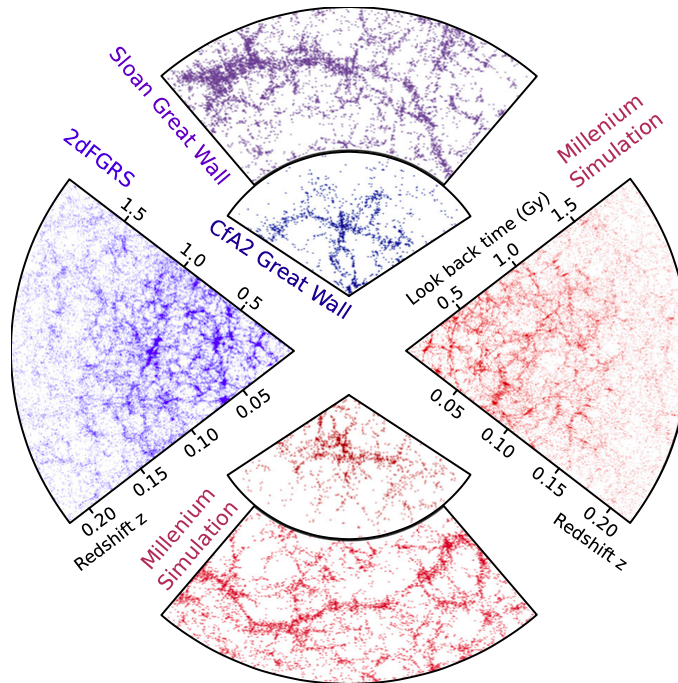


Figure 7 shows an output of the Illustris simulation, with the dark matter distribution on the left panel and the corresponding gas density (main visible matter constituent) on the right.



**Figure 7.** Large scale projection through the Illustris volume at  $z=0$ , centered on the most massive cluster, 15 Mpc/h deep. It shows dark matter density (left) transitioning to gas density (right). Figure from <http://www.illustris-project.org>.

The output of the simulations as the one showed before (there are also others) can be compared to the spectroscopic galaxy survey data from instruments like the 2dF Galaxy Redshift Survey (see figure 8). In this figure large structures, like the Sloan Great



**Figure 8.** Comparison of clustering in observations of galaxy surveys (in blue) and in dark matter simulations (red). From Springel, Frenk & White, Nature **440** (2006) [7].

Wall and the CfA2 Great Wall, are shown in data and compared to the outcome of the Millenium simulation. Very good agreement is found between simulated distributions and measurements in the sense that the degree of structure is equivalent. If dark matter is a particle and it is relativistic at the time of structure formations, the relative size of structures would be smeared out  $\rightarrow$  dark matter can not be 'hot dark matter'. For this reason, we learn from large structures not only that dark matter is necessary to explain the observations but also that it was not relativistic at the time of formation. Therefore we call it 'cold' dark matter in contrast to 'warm' or 'hot' dark matter.

### 1.6. Cosmic microwave background

The cosmic microwave background (CMB) is an isotropic photon emission with a temperature of  $T = 2.7\text{K}$  emitted when the Universe was about 400 000 years old. It was predicted by Gamov 1946 and the first measurement happen only in 1964 when Penzias and Wilson measure it accidentally using horn antennas for telecommunications. Temperature anisotropies in the CMB give us access to the Universe when photons decouple from matter. The first measurement of the anisotropies happened in 1992 by the Cobe satellite which also confirmed the black-body shape of the spectrum. Most precise measurement were performed by the Planck satellite [8] during its operation from 2009 to 2013. [For the students present in the lecture last semester: see CMB lecture.]

Figure 9 (left) shown the map of temperature variations as measured by Planck. Note that the scale of these variations is very small, in  $\mu\text{K}$ . On the right side,

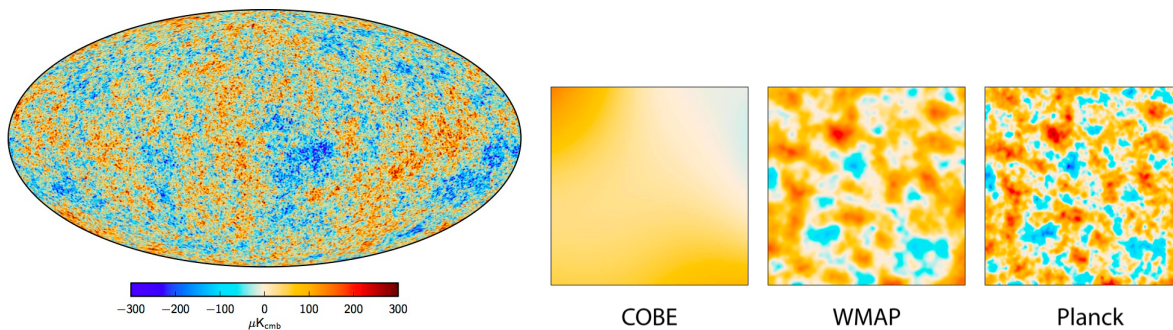


**Figure 9.** Cosmic microwave background maps. (left) Figure Planck Collaboration, arXiv:1507.02704 [11]. (Right) CMB resolution for different satellite measurements (figure from wikipedia).

measurements of Plack in a small region are compared to previous measurements by COBE and WMAP, the improvement in resolution is obvious.

By using the correlation of each two temperatures with respect to the distance between the points, the power spectrum can be calculated (see figure 10). While low  $\ell$ -values in this spectrum correspond to large distances and large  $\ell$  to small ones. For the latter, the resolution of the satellite determines how well structures are measured. The CMB has a characteristic power spectrum with ripples. Oscillations of the baryon-



photon fluid in the gravitational potential dominated by cold dark matter density perturbations in the early Universe give rise to this oscillation pattern in the spectrum (also called acoustic peaks). This power spectrum of temperature fluctuations can

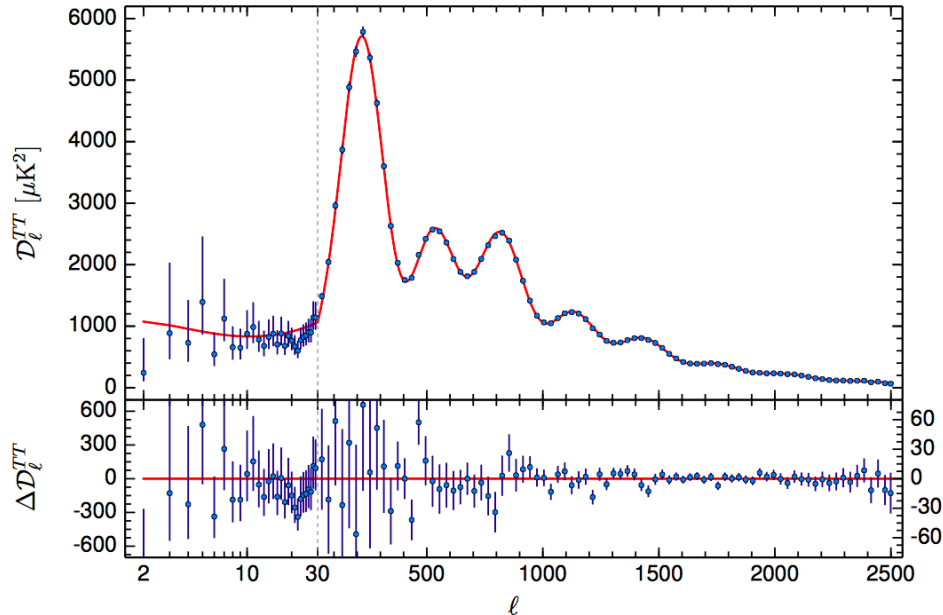


**Figure 10.** Temperature angular power spectrum of the primary CMB map by Planck. Figure Planck Collaboration, arXiv:1502.01589 [13].

be evaluated by a six parameter model which contains, among others parameters, the baryonic matter, dark matter and dark energy contents of the Universe. This cosmological standard model, which fits the data with high significance, is denoted  $\Lambda$ CDM ( $\Lambda$  cold dark matter) indicating that dark matter with a small random velocity is a fundamental ingredient. The  $\Lambda$  refers to the cosmological constant necessary to explain the current accelerated expansion of the Universe [9].

The position of the first peak in the power spectrum determines the curvature of the Universe. From the relative height of these acoustic peaks, the amount of baryonic matter can be estimated, which allows to calculate the total dark matter density in the Universe. Present estimates [10] show a flat Universe with  $\Omega_{\text{DM}} = 0.265$ ,  $\Omega_b = 0.049$  and  $\Omega_\Lambda = 0.686$  representing the densities of dark matter, baryonic matter and dark energy, respectively. Other features in the spectrum are related to how photons were emitted and effects (like lensing) during the propagation. In summary, from CMB we learn not only that dark matter is a necessary constituent in the Universe to explain the emission of this photon background but also that 27 % of the total energy content in the Universe is dark matter.

### 1.7. Summary

In this lecture, some of the most important indications for dark matter have been presented. The hints from Cosmology, CMB measurements and structure formation, are of most relevance but we started with the indications from Astronomy as those are the ones that appear historically first. Note that this is not a complete list, further indications for dark matter appear from comparing the abundances of elements with predictions from Big Bang nucleosynthesis, or from measurements of supernova. In conclusion, we learn that there is evidence for the existence of dark matter at very different scales, from galaxies to the largest structures in the Universe. In the next lecture, we will learn about possible explanations and particle candidates that can account for the observations.

### References

- [1] F. Zwicky, “Die Rotverschiebung von extragalaktischen Nebeln,” *Helvetica Physica Acta* **6** (1933) 110.
- [2] V. C. Rubin, N. Thonnard, and J. Ford, W. K., “Extended rotation curves of high-luminosity spiral galaxies,” *Astrophys. J* **225** (1978) L107.
- [3] A. Einstein, “Lens-Like Action of a Star by the Deviation of Light in the Gravitational Field,” *Science* **84** (1936) 506.
- [4] R. Massey, T. Kitching, and J. Richard, “The dark matter of gravitational lensing,” *Rept. Prog. Phys.* **73** (2010) 086901, [arXiv:1001.1739](#).
- [5] D. Clowe, M. Bradac, A. H. Gonzalez, M. Markevitch, S. W. Randall, *et al.*, “A direct empirical proof of the existence of dark matter,” *Astrophys. J.* **648** (2006) L109, [arXiv:astro-ph/0608407](#).
- [6] D. Harvey, R. Massey, T. Kitching, A. Taylor, and E. Tittley, “The non-gravitational interactions of dark matter in colliding galaxy clusters,” *Science* **347** (2015) 1462, [arXiv:1503.07675](#).
- [7] V. Springel, C. S. Frenk, and S. D. White, “The large-scale structure of the Universe,” *Nature* **440** (2006) 1137, [arXiv:astro-ph/0604561](#).
- [8] **Planck** Collaboration, P. Ade *et al.*, “Planck 2013 results. I. Overview of products and scientific results,” [arXiv:1303.5062](#).
- [9] **Supernova Search** Collaboration, A. G. Riess *et al.*, “Observational evidence from supernovae for an accelerating universe and a cosmological constant,” *Astron. J.* **116** (1998) 1009, [arXiv:astro-ph/9805201](#).
- [10] **Planck** Collaboration, “Planck 2015 results. XIII. Cosmological parameters,” [arXiv:1502.01589](#).
- [11] **Planck** Collaboration, N. Aghanim *et al.*, “Planck 2015 results. XI. CMB power spectra, likelihoods, and robustness of parameters,” [arXiv:1507.02704](#).
- [12] **Planck** Collaboration, R. Adam *et al.*, “Planck 2015 results. X. Diffuse component separation: Foreground maps,” [arXiv:1502.01588](#).
- [13] **Planck** Collaboration, P. A. R. Ade *et al.*, “Planck 2015 results. XIII. Cosmological parameters,” [arXiv:1502.01589](#).
- [14] B. Fields and S. Sarkar, “Big-Bang nucleosynthesis (2006 Particle Data Group mini-review),” [arXiv:astro-ph/0601514](#).